TECHNICAL PAPER

JOURNAL OF THE SOUTH AFRICAN INSTITUTION OF CIVIL ENGINEERING
ISSN 1021-2019 (print) | ISSN 2309-8775 (online)
Vol 68 No 3, September 2026, Pages 2–13, Paper 1898

Effect of aspect ratio and load location on the performance of catenary arches under concentrated loading

D L Teixeira, J E van der Merwe



DAMIANO TEIXEIRA obtained his BEng (2023) and MEng in Structural Engineering (2025) from the University of Pretoria. His interest in funicular structural form began during his final-year research project, which led to the research topic of this paper. His subsequent research focused on timber-concrete composite construction. He is currently employed as a structural engineer at STRENG Consult.
ORCID iD: **0009-0007-0143-9436**

Contact details:
STRENG Consult
475 King's Highway
Lynnwood
Pretoria, 0081
South Africa
damiano@strengconsult.co.za



DR JOHANN VAN DER MERWE (Pr Eng, FSAICE) is a senior lecturer at the Department of Civil Engineering of the University of Pretoria. He completed his BEng and MSc (Eng) degrees at Stellenbosch University and his doctorate at the Swiss Federal Institute of Technology in Zürich, Switzerland. He worked as a consulting design engineer in South Africa and New Zealand before joining the University of Pretoria in 2023. His main research focus is in the field of timber structural engineering.
ORCID iD: **0000-0003-1748-0461**

Contact details:
Department of Civil Engineering
University of Pretoria
Hatfield
Pretoria, 0002
South Africa
vandermerwe.johann@up.ac.za

Catenary arches represent an efficient structural form under self-weight, as they can develop pure compression with minimal bending. In practice, however, arches are often subjected to pattern loading and/or concentrated loads, which alter the theoretical thrust-line geometry and introduce bending moments.

This study investigates the influence of arch span-to-depth ratio and load position on the structural response of catenary arches subjected to concentrated loading. Two arch geometries with aspect ratios of 0.35 and 0.60 were tested experimentally under both central and eccentric point loads. Observed hinge formation and ultimate load-carrying capacities were compared with theoretical thrust-line calculations and results from simple linear elastic numerical analyses. The results show that arches can sustain higher loads when the concentrated load is applied at the apex rather than eccentrically. This influence of load position was found to be more pronounced for shallower arches.

The study compares experimental observations of hinge locations with locations estimated from theoretical thrust-line geometries and maximum bending moments from simplified linear elastic numerical models. It is shown that such simplified methods are adequate for estimating hinge locations even beyond the initial elastic response range.

Keywords: catenary arch, thrust line, optimised structural form, eccentric loading, hinge formation.

INTRODUCTION

Catenary arch structures are the optimal structural forms for ensuring pure axial force without induced moments over a span under self-weight (Allen & Zalewski 2009; Hawkins *et al* 2019). This is especially favourable for concrete arches, which are well-suited to form compression elements. As such, this form is often used in bridge construction (e.g. Figure 1) and has also been proposed for floor construction to reduce the amount of concrete material and, as such, embodied carbon (e.g. Figure 2). Vaulted structures designed by Heinz Isler highlight the extent to which concrete volume can be reduced when roof structures are built to follow catenary forms (e.g. Figure 3).

Robert Hooke described the optimal form of a structure spanning a horizontal distance under its own weight as that of a hanging chain – a structure in pure tension. Inverting this hanging form yields the shape of a catenary arch, which is in constant compression under its own weight. Such lines, which define the shape of constant compression, are called thrust lines (also known as the funicular form). It is, however, Rene Descartes who is credited for establishing a connection between such a curve's construction and its algebraic equation in 1637 (Cvetković *et al* 2021). The geometry of this hanging chain catenary can be described according to Equation 1 (Block *et al* 2006).

$$y = a \cdot \cosh\left(\frac{x}{a}\right) \tag{1}$$

Where:
- y = vertical height of the catenary
- x = horizontal distance from the centre of the catenary apex
- a = scaling factor that dictates the proportional shape (span/height) of the catenary.

Teixeira D L, Van der Merwe J E. Effect of aspect ratio and load location on the performance of catenary arches under concentrated loading. J. S. Afr. Inst. Civ. Eng. 2026:68(3), Art. #1898,12 pages. http://dx.doi.org/10.17159/2309-8775/2026/v68n3a1

The *Journal of the South African Institution of Civil Engineering*, which is distributed internationally, is a peer-reviewed, open-access journal licensed under a Creative Commons Attribution Licence (CC BY-NC-ND). Readers may therefore freely use and share the content as long as they credit the original creator and publisher, do not change the material in any way, and do not use it commercially. Copyright of this article remains with the authors.



Figure 1 The Salginatobel bridge in Switzerland was designed by Robert Maillart, who formed the arch according to thrust line patterns (Rama 2008)



Figure 2 Vaulted slab designed to minimise material use (Oval *et al* 2023)



Figure 3 Heinz Isler is renowned for the design of several thin vaulted structures, such as this garden centre in France (Boller *et al* 2024)

This concept has not only been used as the reference for some arch structures, but also for the analysis of domes (Figure 4) and vaulted structures (Figure 5) over centuries. It has also been shown that catenary theory can be used for the analysis and design of ordinary reinforced concrete beams (Gohnert & Bradley 2023).

Therefore, as long as the geometry of an arch centreline follows theoretical thrust lines, the arch can be expected to be in pure compression. Deviation of structural form from this thrust line geometry will, however, result in eccentric loading and, in turn, bending moments. If the flexural capacity of the arch cross-section is not capable of resisting such resulting bending moments, hinges will form. This is especially critical, for example, for stone masonry arches. Gáspár *et al* (2023) illustrate how the location and number of hinges that form in such masonry arches depend on the extent of arch geometry deviation from theoretical thrust lines (Figure 6).

The funicular form of a structure (i.e. the theoretical thrust line geometry) under loading that differs from uniform self-weight loading differs from the classical catenary form. Following Simon Stevin's description of masses suspended from a hanging chain in 1586, and Pierrre Varignon's description of force polygons in 1725, Karl Culmann is credited as the first to formalise the method of graphic statics to analyse funicular structures under applied concentrated loads (Block *et al* 2006). While a hanging chain model

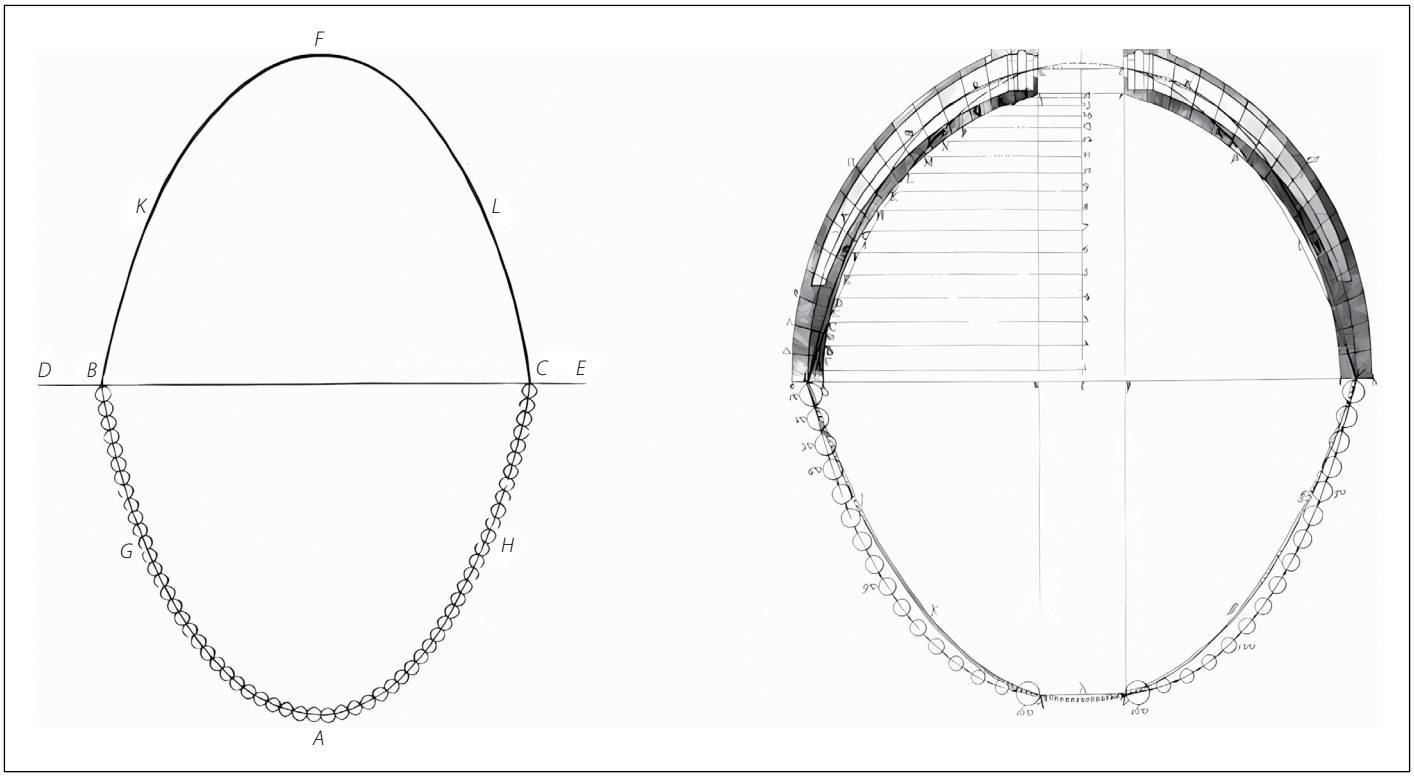


Figure 4 Giovanni Poleni based his analysis of domes on Robert Hooke's hanging chain analogy of catenary form (Poleni 1748, as cited in Jannasch 2017)



Figure 5 Bradley and Gohnert (2016) used this hanging chain model to describe the inverted catenary form of a vaulted structure

might still be considered to represent the funicular shape for a structure exposed to concentrated loads, it is clear that the resulting thrust line form differs from that under uniform self-weight loading (Figure 7). Such concentrated loads may result, for example, when arches support columns or when moving imposed axle loads are applied (e.g. bridge structures).

Similarly, when pattern loading must be accounted for, several theoretical thrust lines may develop. If flexural effects due to eccentricity between the arch element centre line and the theoretical thrust line are to be minimised, the structural depth must be sufficient to resist bending moments due to eccentricities between the structure's geometry and theoretical thrust lines (e.g. Figure 8). This was, for example, considered by Robert Maillart when he designed the arch of the Salginatobel bridge (Figure 9).

Analytically similar to masonry arches, hinges might form in reinforced concrete arches under the application of point loads if the resulting bending moments exceed the flexural capacity of the section. The number of hinges that might form in an arch, therefore, depends on the arch geometry, the position of an eccentric load, and the flexural capacity of the material (Bradley 2021).

While several studies have investigated simple analysis techniques for catenary arches under self-weight in the elastic range up to hinge formation (e.g. Block *et al* 2006, De Bruin 1996, Zhang *et al* 2024), few have explored the practical relevance of such analyses for identifying the successive locations of hinge formation in concrete arches (e.g. Gáspár *et al* 2024). Moreover, the performance of catenary arches under concentrated point loads is often investigated in the context of masonry arches, where pure hinge formation is more likely than for reinforced concrete arches. The extent to which arch geometry influences structural response and hinge formation of concrete arches under such concentrated loading conditions has received comparatively little experimental attention.

Since concentrated loads alter the theoretical thrust line geometry from the classical catenary form, different arch aspect

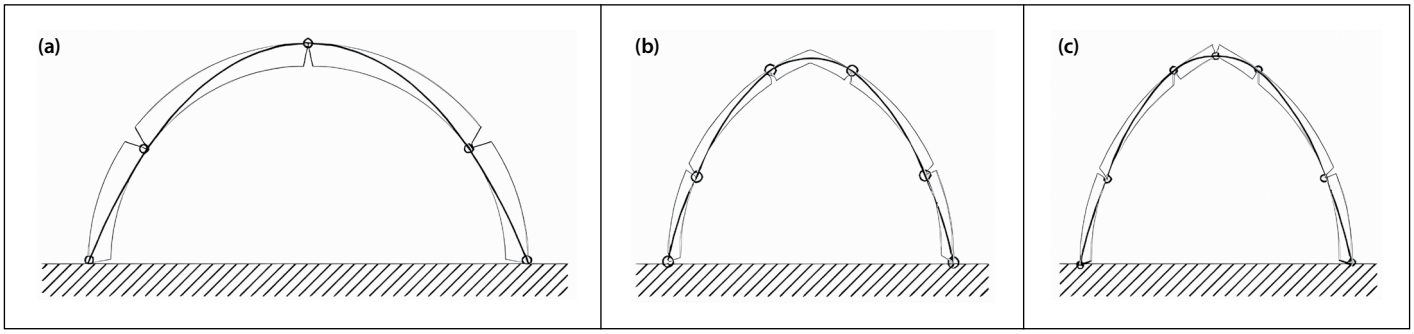


Figure 6 The extent to which arch geometry and theoretical thrust lines differ will determine the location and number of hinges that might form in masonry arches; in this case, (a) 5, (b) 6, or (c) 7 hinges (adapted from Gáspár *et al* 2023)

ratios may perform differently depending on the load position. This study aims to test this hypothesis by investigating arches with two aspect ratios under central and eccentric loading. Geometric deviations from theoretical thrust lines are compared with the positions of crack development and propagation identified from experimental tests.

In addition to evaluating the extent to which the capacity at first hinge formation differs, the study investigates how well a design engineer might identify hinge-formation locations using simple linear elastic analysis methods, as well as the limitations of relying on such simplified methods. The objective of this study is to evaluate the ability of theoretical thrust-line analysis and numerical modelling to predict the location of hinge formation in concrete arches subjected to concentrated loading. Although the applied loads corresponding to hinge formation are reported, the study does not seek to quantitatively evaluate arch member capacities. Conventional flexural stress calculations developed for horizontally spanning beam members are not directly applicable to arches under concentrated loading, where the internal stress state is strongly influenced by combined axial compression, bending, and local stress redistribution.

SCOPE AND METHODOLOGY

To investigate two aspect ratios, concrete arch heights were varied over a 1 m horizontal distance. This section discusses the concrete material, sample preparation, and experimental setup.

Concrete material

A high-strength steel fibre reinforced concrete mixture (developed by Weyers 2020) was used for all arch specimens. Although the strength of such arches lies in their geometry and not high material strength demands, this concrete mixture was used to ensure that small-scale samples could be produced with good quality control during sample preparation, to avoid detrimental drying, shrinking cracks, and damage during demoulding and handling of samples in the laboratory. Moreover, this was deemed an appropriate deviation from potential full-scale structures given the comparative nature of the study's aim and objectives.

In addition to casting arch specimens (tested 14 days after casting), cube and cylinder samples were prepared to determine the material properties at 14 days, including compressive strength ($f_{c,14}$), modulus of elasticity ($E_{c,14}$), and splitting tensile strength ($f_{t,14}$). After casting, arches were left to cure in ambient laboratory conditions (approximately 25°C and 55% relative humidity) while covered with a plastic sheet. To ensure representative results, the

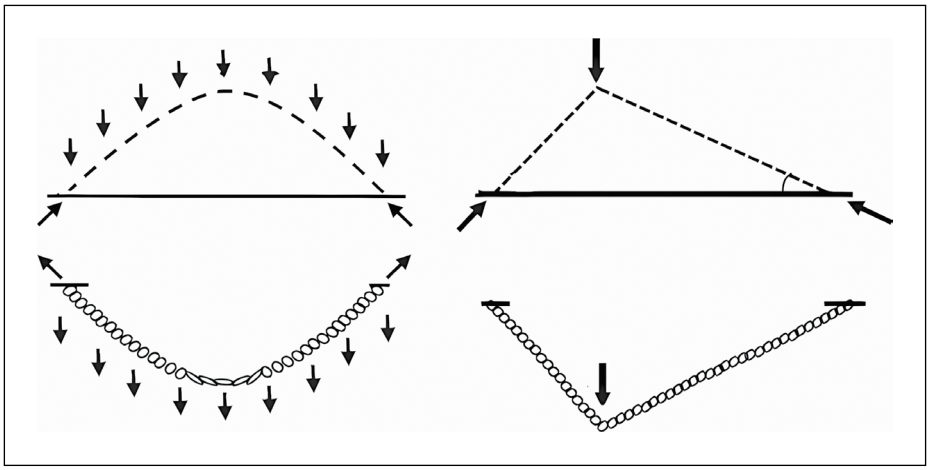


Figure 7 The hanging chain analogy describes the thrust line geometry under self-weight (left) and under applied concentrated loads (right) (adapted from Gohnert & Bradley 2023)

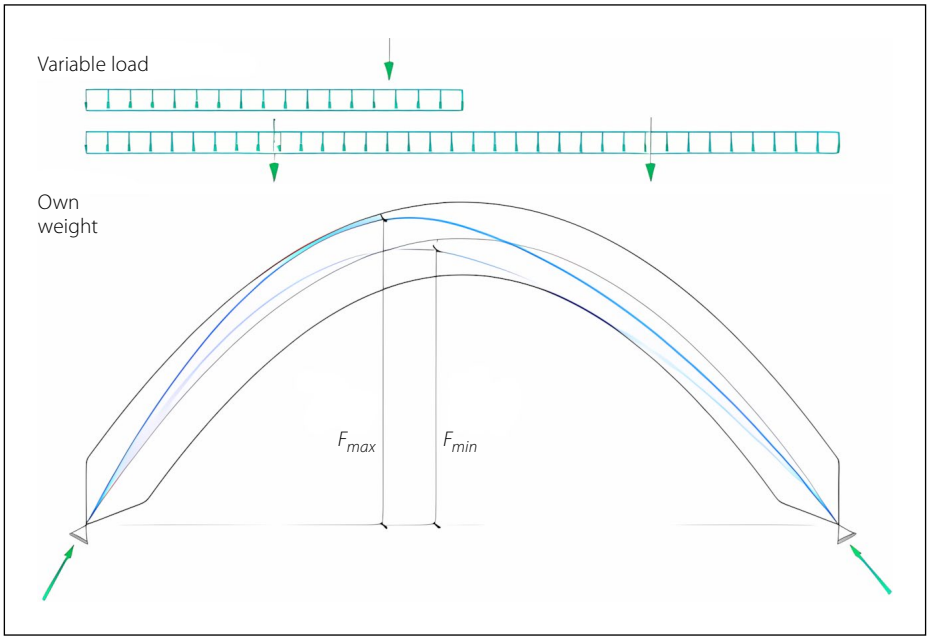


Figure 8 Under the application of variable loads, an arch element should be of sufficient depth to encapsulate the thrust lines resulting from maximum (F_{max}) and minimum (F_{min}) loads

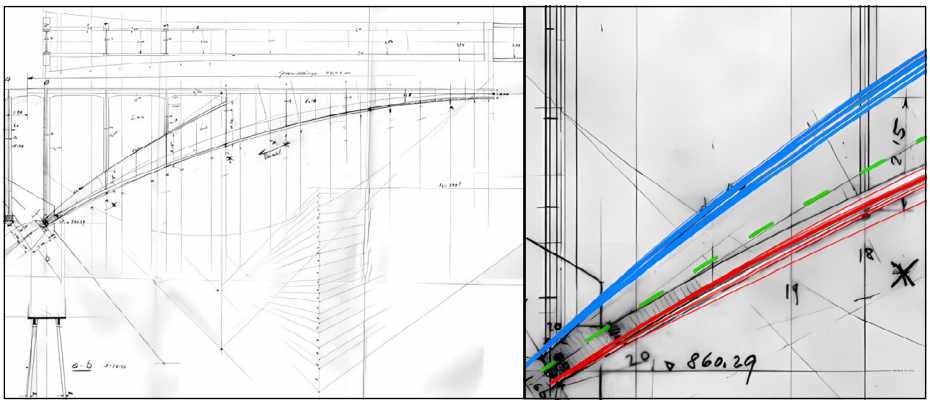


Figure 9 Robert Mallart's working drawing of the Salginatobel bridge with graphic statics calculations (left). The upper (blue) and lower (red) thrust lines (right) due to pattern loading on the bridge deck are all encapsulated in the depth of the arch to avoid excessive flexural effects (adapted from Fivet & Zastavni 2012)

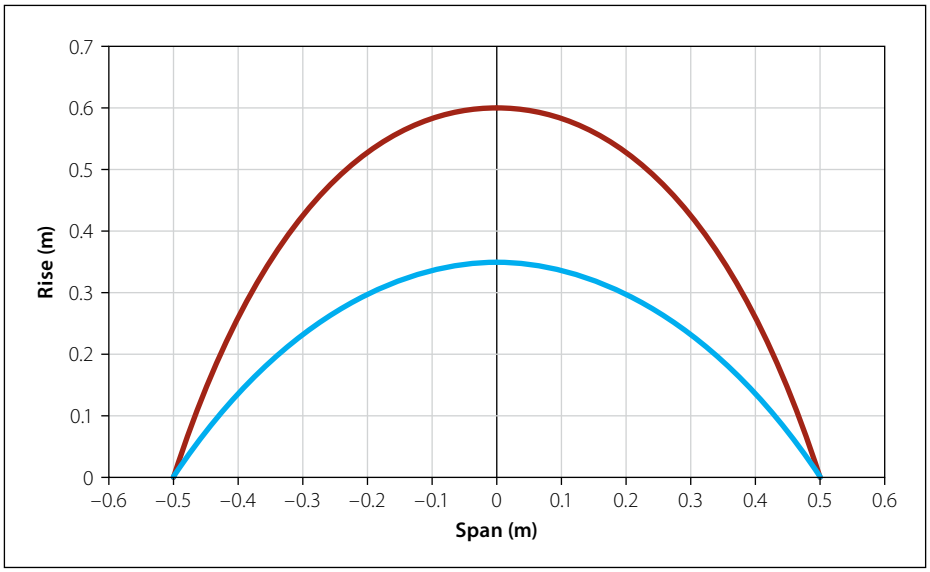


Figure 10 A steep arch and a shallow arch (aspect ratios 0.60 and 0.35, respectively) were investigated

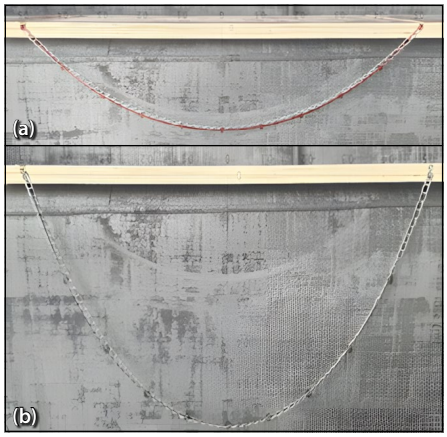


Figure 11 The calculated coordinates of the catenary arch geometries (both (a) shallow and (b) steep) match the shape of hanging chains well

Table 1 Concrete mixture considered in this study

Material	kg/m^3	Relative density
Cement – CEM I 52.5R	542	3.14
Silica fume	146	2.45
Fly ash	146	2.22
Dolomite sand < 4.75 mm	1005	2.85
Dolomite stone < 9.5 mm	251	2.91
Silica sand < 1.5 mm	216	2.67
Superplasticiser Optima 100 Chryso	25.6	1.06
Water	146	1.00
Short steel fibres – 30 mm hooked end	149	7.85

Table 2 Reference concrete properties

	$f_{c,14}$ / $f_{c,28}$ [MPa]	$E_{c,14}$ [GPa]	$f_{t,14}$ [MPa] Pre-crack (post-crack)
Mean	131.5 / 139.1	46.49	7.02 (10.90)
St. dev	4.15 / 3.14	1.61	0.59 (2.75)
CV	0.032 / 0.023	0.035	0.084 (0.252)

CV = coefficient of variation
St. dev = Sample standard deviation

concrete samples for 14-day testing were cured in the same conditions as the arch samples. A set of concrete cubes was also prepared to validate the reference 28-day compressive strength ($f_{c,28}$). Table 1 summarises the concrete mix proportions, while Table 2 summarises the recorded material properties.

Arch geometries

Spanning 1 000 mm, two arch depths were considered to obtain span-to-depth ratios of 0.35 and 0.60 (i.e. arch centreline heights of 600 mm and 350 mm, respectively).

Equation 1 was used to determine the catenary shapes of the two arches, with centreline geometries shown in Figure 10. The geometries match those of physical hanging chain models well (Figure 11). Scaling factors of a = 0.2733 and a = 0.4049 were determined for the steep and shallow arch geometries, respectively.

Custom moulds were constructed to cast the arch geometries. The cross-sectional dimensions of the arches were 160 mm wide and 50 mm thick. Although this thickness might be considered proportionally greater than what would be relevant to full-scale structures of this nature (where the aim is to reduce material volume), it ensured robust samples that avoid drying shrinkage and limit possible damage during handling. Moreover, since the study focuses on a comparison of the effects of geometry and load position up to the point of hinge formation, and not on quantitative effects beyond the linear elastic range, this was deemed adequate.

Figure 12 shows the two arch geometries that were produced. For each arch aspect ratio, one was cast with a smooth upper finish for loading at the apex. One arch of each aspect ratio was cast to apply a concentrated load 200 mm from the centre line. To accommodate the load application in this (inclined) position, an additional volume of concrete was added, connected to the arch with reinforcement dowels, and finished to ensure a horizontal top surface. This localised thickening of the concrete section increased the section's stiffness over this 50 mm length. Although experimental observations show the relevance of this effect on a localised level, it did not appear to have a substantial effect on global arch behaviour.

Experimental setup

Arches were placed on two metal plates with a lubricated interface to provide vertical support while minimising horizontal friction. Rigid horizontal restraints were placed at both supports, with a load cell at one support to record horizontal thrust (Figure 13a).

A displacement-controlled load was distributed over the full width of the arches to simulate quasi-static loading. The side faces of the arches were painted white

and partially sprayed to carefully monitor displacements and crack formation with photos taken at 10-second intervals, as shown in Figure 13b.

When a load was applied at the apex of the arches, a linear variable differential transformer (LVDT) measured the vertical displacement of the soffit at the apex. Due to practical constraints, LVDTs could not be placed directly under the off-centre loading location. In these cases, displacement at the load application was recorded directly from the calibrated hydraulic actuator.

Numerical comparison model

Experimental observations were compared to results from simple linear elastic analyses in Prokon (Prokon Software Limited 2025). The arch geometry was discretised using nodes spaced at 10 mm horizontal intervals along the span, and vertical coordinates calculated according to Equation 1.

To validate the numerical model, theoretical calculations were compared to model output under arch self-weight only. A constant horizontal thrust is expected under self-weight only. It is shown in the appendix that the theoretical constant thrust can be calculated according to Equation 2.

$$H = w \cdot a \tag{2}$$

Where:

H = horizontal thrust
w = self-weight of the reinforced concrete cross-section
a = scaling factor that dictates the proportional shape (span/height) of the catenary.



Figure 12 Steep and shallow arch geometries with the formwork required for the bearing surface for the eccentric load application

Assuming a unit self-weight of 25 kN/m^3 for validation purposes, the theoretical constant thrust amounts to H = 0.055 kN for the steep arch, and H = 0.081 kN for the shallow arch. Two-dimensional linear elastic analyses yielded the same horizontal reaction and horizontal axial force at the apex of each arch, where the internal axial force is horizontal.

The axial force in each of the arch geometries was compared to theoretical values at the apex, at supports, and at the quarter span. It is shown in the appendix that the axial force is related to the catenary arch geometry according to Equation 3.

$$N = H \cdot \sqrt{1 + \sinh^2\left(\frac{x}{a}\right)} \tag{3}$$

Where:

N = axial force
x = horizontal position measured from the apex.

Table 3 compares the results. Linear elastic analysis output agreed well with theoretical axial force values, with a maximum difference of 1% observed for the shallow arch. This suggests that the numerical model can adequately analyse catenary behaviour in the elastic range.

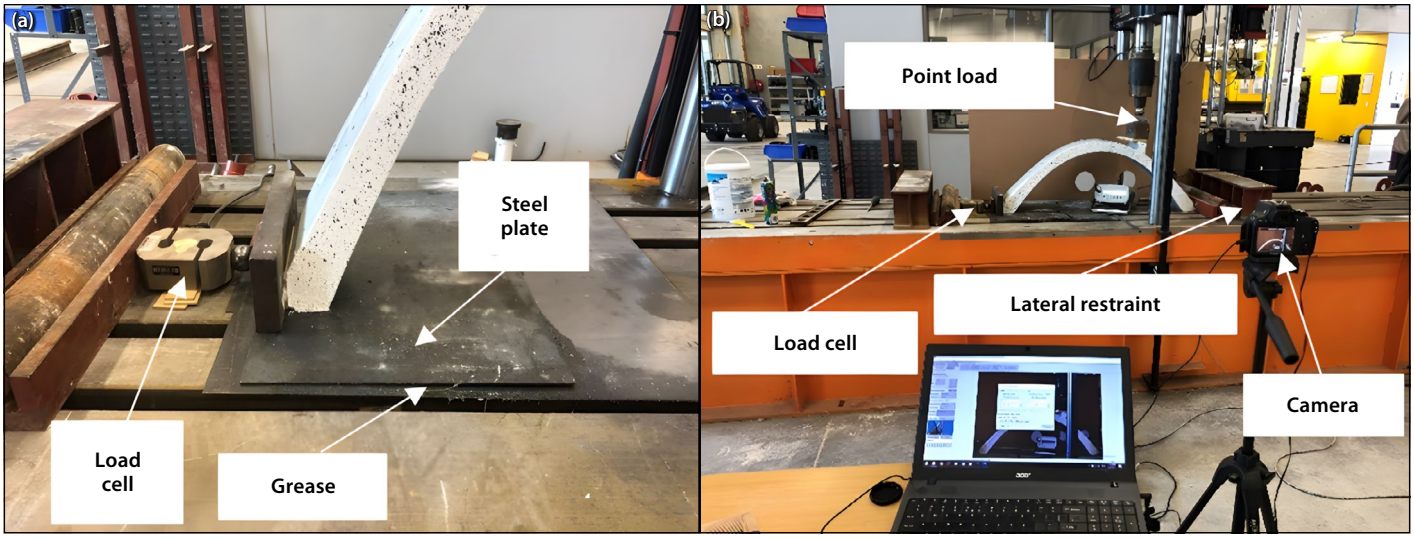


Figure 13 (a) Supports were provided to record the horizontal thrust; (b) The experimental setup comprised displacement-controlled load application and continuous monitoring

Table 3 Comparison of theoretical values for the axial force along the arch geometries with output from linear elastic analyses under self-weight only

Arch	Position	Theoretical value	Analysis output
Steep arch	Support	0.175 kN	0.175 kN
	Quarter span	0.079 kN	0.079 kN
	Apex	0.055 kN	0.055 kN
Shallow arch	Support	0.151 kN	0.149 kN
	Quarter span	0.097 kN	0.097 kN
	Apex	0.081 kN	0.081 kN

RESULTS AND DISCUSSION

The arches' behaviour during experimental testing was characterised by the formation of flexural cracks at locations where the thrust line deviated from the arch geometries. These cracks developed progressively until successive hinge formations ultimately led to collapse. The capacity and failure modes are compared in this section. Theoretical locations of hinge formation are compared to experimental observations and linear elastic analyses. Although the location of the maximum bending moment obtained from such linear elastic analyses should agree with the location of the maximum deviation from theoretical thrust lines and the locations of hinge formation from experimental observations, it does not allow comparison with experimental load-deflection behaviour beyond the elastic range. Such analyses do not capture the development and spread of crack formation leading up to final collapse. Differences in the ultimate capacity between a linear elastic analysis and experimental observations are therefore anticipated.

Performance under central load

With concentrated loads applied at the apex of the arches, initial cracks were observed at the apex at applied loads of 20 kN and 25 kN for the steep and shallow arches, respectively. When these concentrated loads are applied to the numerical models, maximum moments of 1.43 kNm and 1.57 kNm are obtained at the apex of the steep and shallow arches, respectively. Axial compressive forces at the apex amounted to 6.19 kN and 13.60 kN for the steep and shallow arches, respectively. The bending moments differ by only 9%, while the resulting tensile

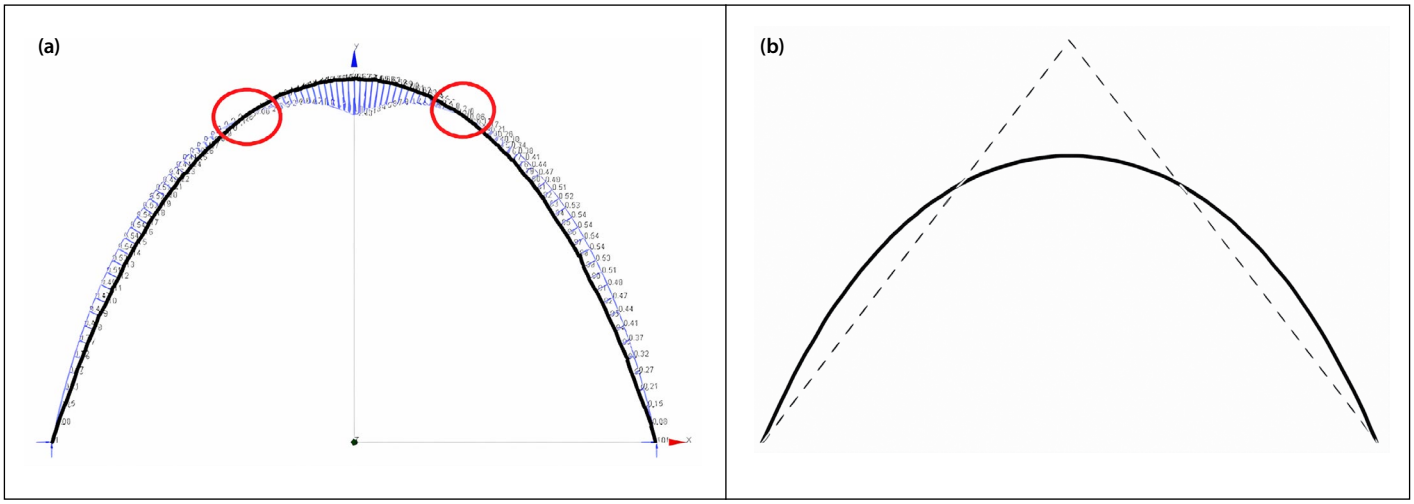


Figure 14 Considering the points of contraflexure from the bending moment diagrams of the arches under central loading (a), as the position where theoretical thrust lines should pass through the arch geometry (b), the maximum deviation between thrust line and arch geometry is observed to be at the apex

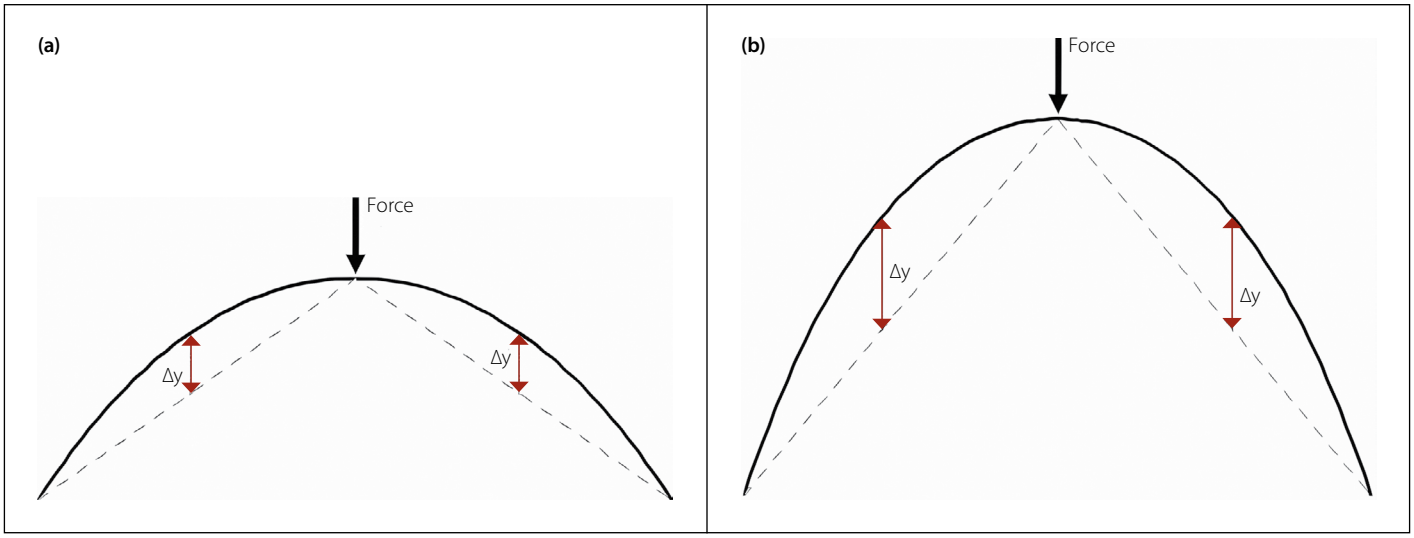


Figure 15 Arch geometry and theoretical thrust lines under central point loading for the shallow arch (a) and steep arch (b). The maximum vertical deviation (Δ*y*) is notably more for the steep arch than for the shallow arch

stresses from combined axial and flexural effects differ by only 5%. The difference in applied load at initial hinge formation, therefore, appears to correspond to similar section capacities. Moreover, the maximum deviation between the theoretical thrust line and the arch geometries prior to hinge formation is at the apex (Figure 14).

Following flexural crack formation at the apex, the linear elastic model was changed from a two-hinge arch to a three-hinge arch, i.e. an arch that now has hinges at the two supports as well as at the apex. Figure 15 compares arch geometries and theoretical thrust lines for concentrated loads, assuming a hinge at the apex. The maximum vertical deviation was calculated to be 179 mm (280 mm horizontally from the apex) and 96 mm (260 mm horizontally from the apex) for the steep and shallow arches, respectively. From Figure 16, it follows that the magnitude of the bending moment imposed in the arch is equal to the product of the (constant) horizontal thrust and this vertical deviation, i.e. $M = H \cdot \Delta y$.

The positions of maximum bending moments obtained from the two-dimensional linear elastic analyses agreed with the theoretical positions of maximum vertical deviation between the thrust line and the arch geometry (Figure 17).

The steep arch finally resisted a maximum load of 25 kN, while the shallower arch resisted a maximum load of 37 kN. Figure 18 shows the arches after failure under a central point load at the apex.

Final hinges were observed to form at positions from the apex that corresponded to the maximum vertical deviation between the theoretical thrust lines and the arch geometry, as well as to the associated

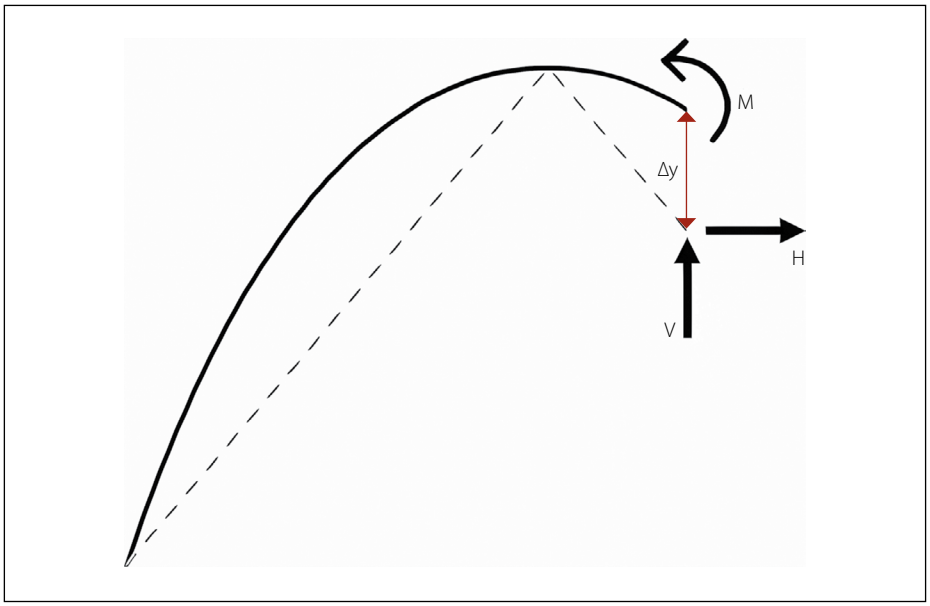


Figure 16 At any given section along the arch, the flexural moment (M) is equal to the constant horizontal thrust (H) multiplied by the vertical difference (Δy) between the arch and the theoretical thrust line

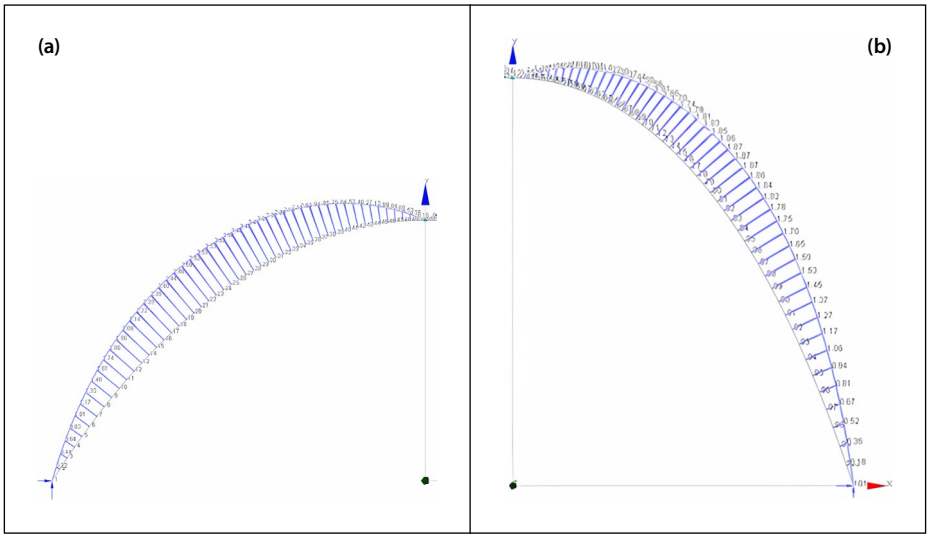


Figure 17 The maximum bending moments obtained from linear elastic analyses of a three-hinge (a) shallow arch and (b) steep arch aligned with the location of maximum vertical deviation between theoretical thrust lines and arch geometries



Figure 18 Both the shallow arch (a) and steep arch (b) formed a five-hinge failure mechanism

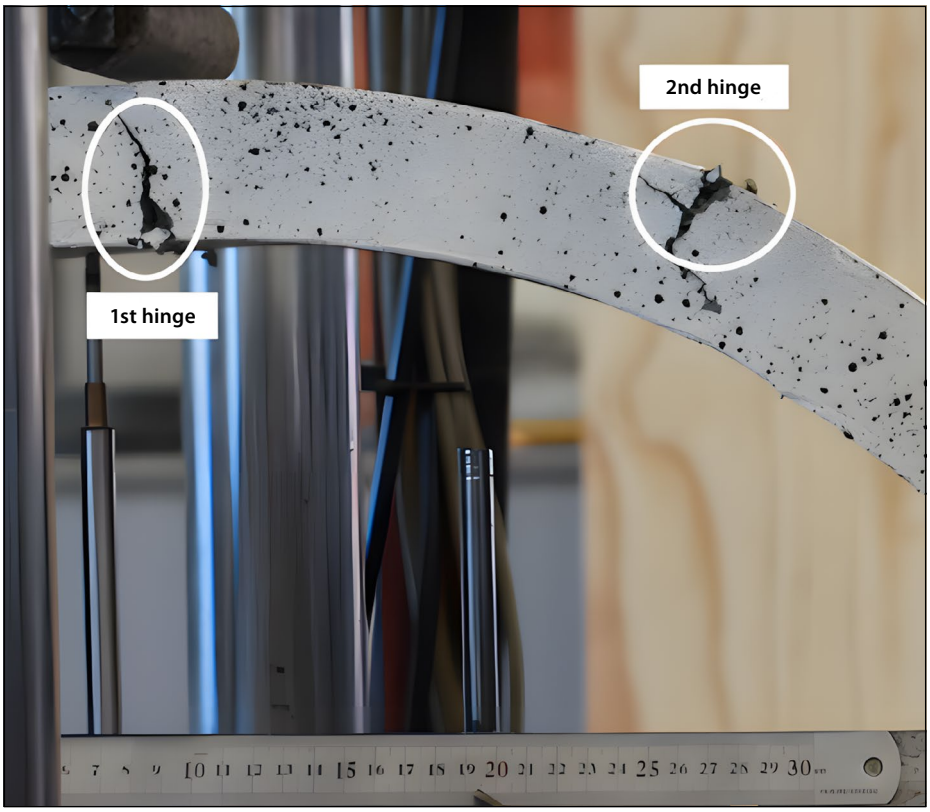


Figure 19 After the first hinge formed at the apex, a second hinge formed at a location that matched theoretical calculations (in this case, 260 mm from the apex for the shallow arch)

Table 4 Comparison of the location of hinge formation under central loading measured horizontally from the apex

	From flexural cracks observed from experimental tests	From maximum deviation from thrust line	From maximum bending moment in numerical analyses
Steep arch First hinge	0 mm	0 mm	0 mm
Steep arch Subsequent hinge	270–280 mm	280 mm	270–290 mm
Shallow arch First hinge	0 mm	0 mm	0 mm
Shallow arch Subsequent hinge	260–270 mm	260 mm	260–270 mm

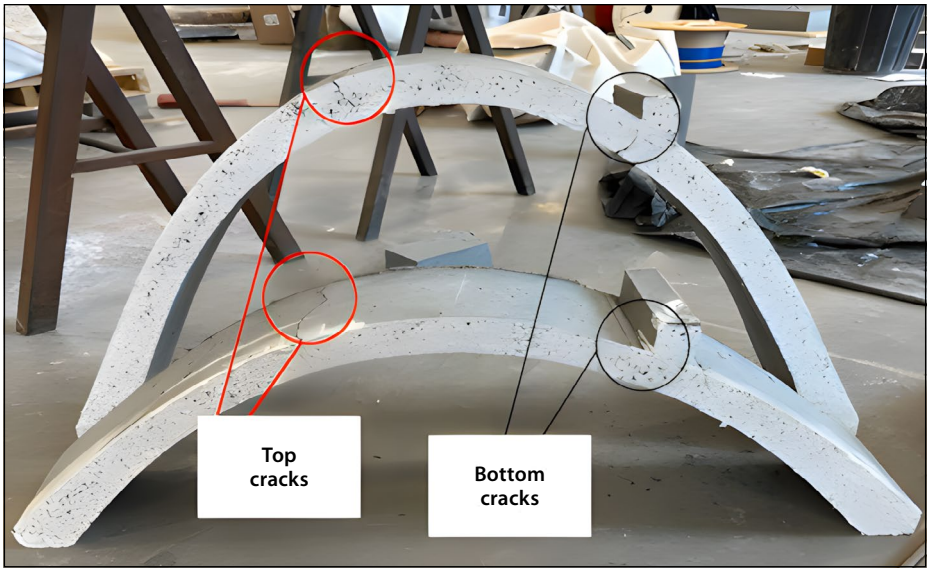


Figure 20 Arches loaded off-centre after failure

maximum bending moment (Figure 19). The tensile stress at the hinge locations was calculated as the combined effect of flexural stress and axial compression from the linear elastic analyses of the three-hinge model when the maximum experimental concentrated loads were applied at the apex. This resulted in a tensile stress in the shallow arch that is 23% greater than that in the steep arch and substantially greater than the concrete's splitting tensile strength. This discrepancy may be attributed to residual flexural stiffness at the apex, as a perfect hinge (assumed in the numerical model) is unlikely in the experimentally tested specimens. This highlights that such simplified analyses might not be sufficient to assess the extent of capacity after initial flexural cracks appear. In contrast, and as shown in Table 4, such simplified analyses might be considered sufficient for identifying the location of hinge formation.

Performance under eccentric loads

Both arch geometries were loaded at a position 200 mm away from the apex. Figure 20 indicates where loads were applied, and shows the position of crack formation after failure.

Both arches resisted very similar ultimate loads, with the steep arch resisting a maximum load of 20 kN and the shallow arch 21 kN. Moreover, the hinge locations seem to agree well between the two arches, first forming near the position of the applied load, and then at similar locations on the opposite side of the apex. This agrees with a comparison of linear elastic analyses of an eccentrically applied point load on both the shallow and steep arches. As shown in Figures 21 to 24, the locations of maximum bending moments obtained from elastic analyses agree with the locations of maximum vertical deviation between arch geometries and theoretical thrust lines. This supports the use of simple elastic analysis as a practical tool for predicting likely hinge locations. It should be noted that bottom cracks did not form directly below the applied load, but rather at the edge of the additional concrete volume added to accommodate load application. This is most likely due to the increased stiffness resulting from the localised thicker section.

The location of the maximum moment that develops in the three-hinge shallow and steep arches was found to differ by approximately 20 mm. The maximum vertical deviation between theoretical thrust lines and arch geometries at these locations, however, is approximately 1.7 times greater for the steep arch than for the shallow arch.

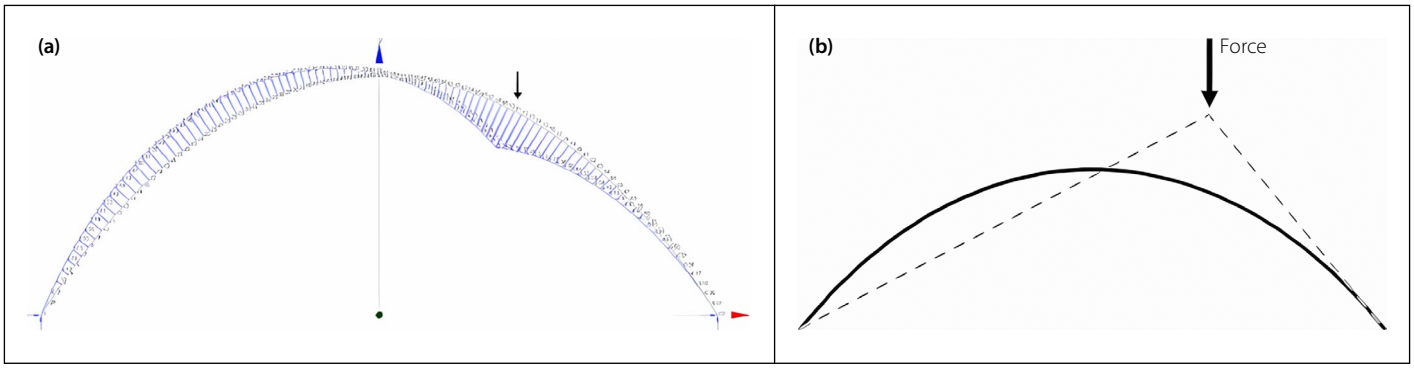


Figure 21 The position of maximum bending moments (a) for the two-hinge shallow arch under eccentric loading agrees with the locations of maximum deviation between the arch geometry and the theoretical thrust lines (b)

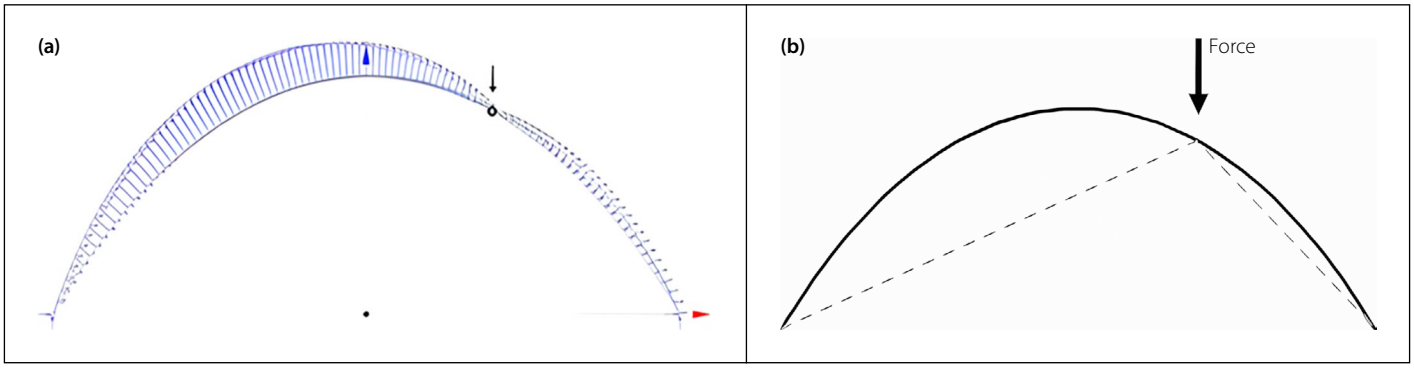


Figure 22 The position of maximum bending moments (a) for the three-hinge shallow arch under eccentric loading agrees with the locations of maximum deviation between the arch geometry and the theoretical thrust lines (b)

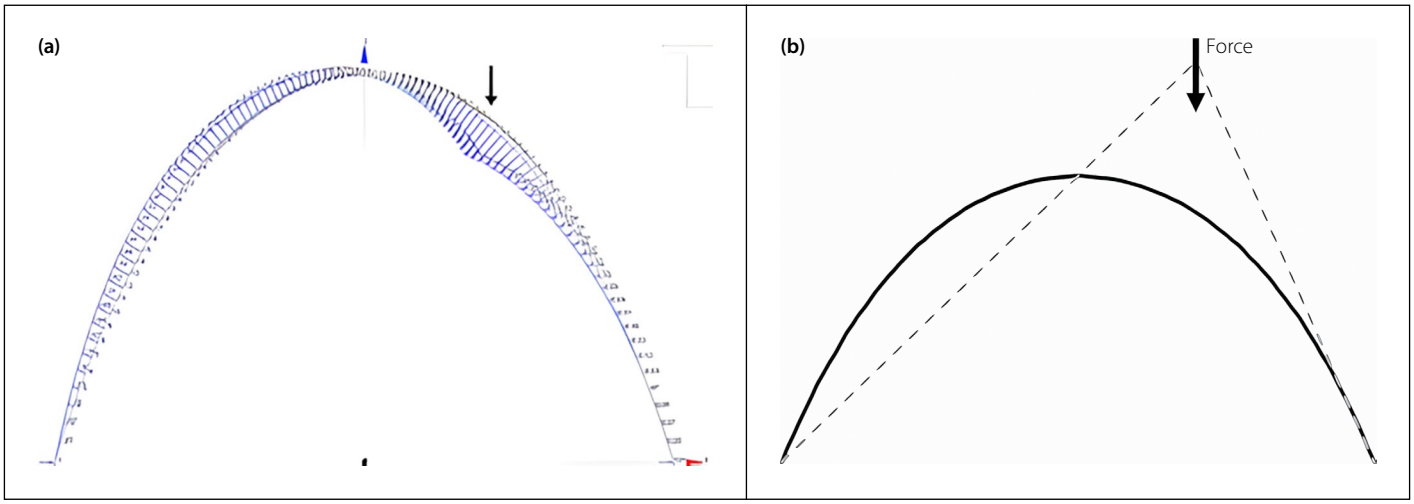


Figure 23 The position of maximum bending moments (a) for the two-hinge steep arch under eccentric loading agrees with the locations of maximum deviation between the arch geometry and the theoretical thrust lines (b)

This, together with a lower axial compressive force identified from linear elastic analyses at this position, suggests that the steep arch should experience substantially more flexural tensile stress under the same level of eccentrically applied load than the shallow arch. This prediction was not observed experimentally, where a pure hinge did not form at the point of applied load. Similar to concentrated loads applied to the apex of the arches, the simple linear elastic analyses appear to accurately identify the locations of hinge formation, even after first (partial) hinge formation (see Table 5 for a

Table 5 Comparison of the location of hinge formation under eccentric loading measured horizontally from the apex

	From flexural cracks observed from experimental tests	From maximum deviation from thrust line	From maximum bending moment in numerical analyses
Steep arch First hinge	175 mm	200 mm	200 mm
Steep arch Subsequent hinge	130 mm	190 mm	170-180 mm
Shallow arch First hinge	175 mm	200 mm	200 mm
Shallow arch Subsequent hinge	200 mm	170 mm	170-190 mm

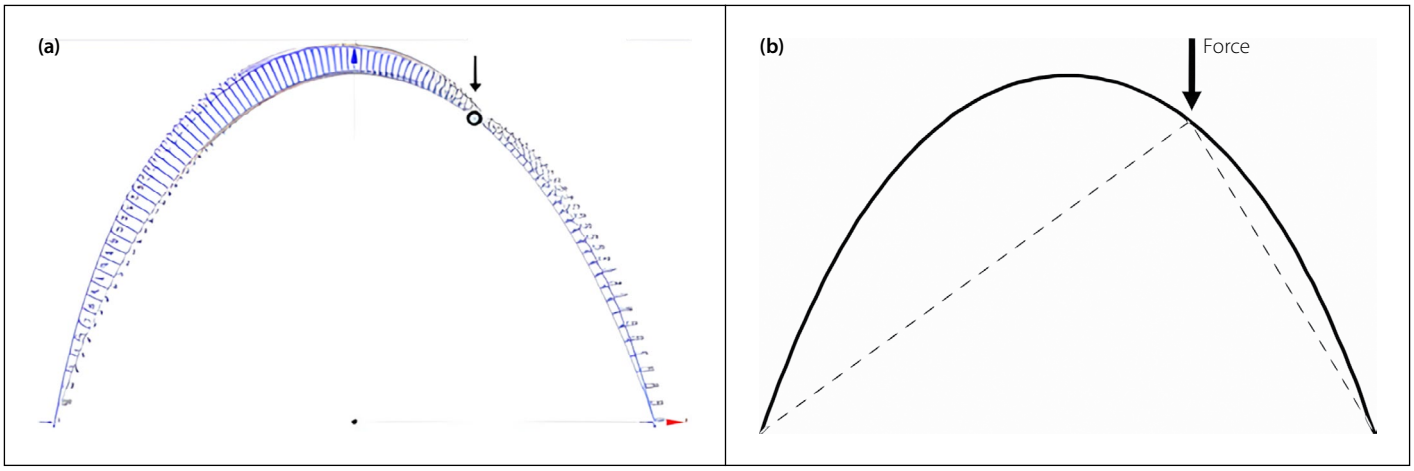


Figure 24 The position of maximum bending moments (a) for the three-hinge steep arch under eccentric loading agrees with the locations of maximum deviation between the arch geometry and the theoretical thrust lines (b)

comparison of hinge locations), but not the ultimate capacity in this nonlinear regime.

Comparison of load position and arch geometry

A comparison of the ultimate capacities of the four arches (steep and shallow arches, with loads applied at the apex and eccentrically) should ideally account for the likely spread of results, especially since the response extends into a nonlinear regime. Since only one arch of each configuration was tested, an approximate range of values was estimated based on the coefficient of variation observed in material property tests (Table 2). Assuming a coefficient of variation of 0.20 to approximately match tensile strength material property tests, the standard deviation, and subsequent upper and lower bounds of a likely 95% confidence interval around observed values were calculated. Results are compared in Figure 25.

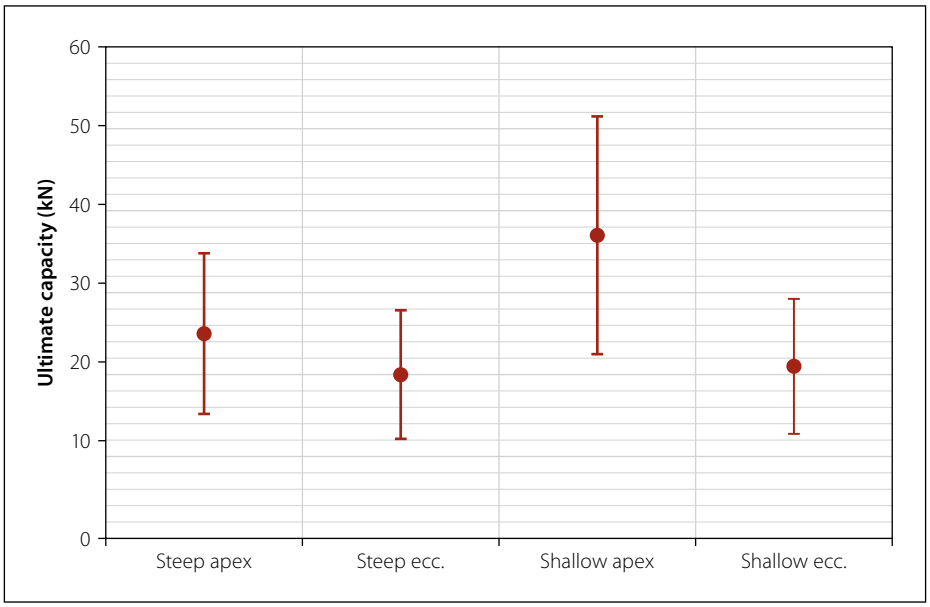


Figure 25 Ultimate capacity against applied load for the shallow and steep arches with loads applied at the apex and eccentrically. Error bars indicate the likely upper and lower bounds of the 95% confidence interval

A comparison of results highlights that eccentric loading reduces the ultimate load-carrying capacity. This agrees with the general understanding of arch behaviour that greater deviation between arch geometry and theoretical thrust lines results in greater flexural effects. Experimental studies reported in the literature seem to support this observation. Liu *et al* (2025) have shown that arches subjected to asymmetric loading exhibit significantly lower ultimate capacity than under symmetric loading, due to increased bending and cracking near the load location.

Where a concentrated load is applied to the apex of the arches, the shallow arch resists a greater ultimate load. This is likely due to the greater horizontal thrust that counters flexural tensile stresses. Results reported elsewhere have shown that the optimal arch form under point loads tends toward shallower geometries as loading increases, reflecting the beneficial effects of greater horizontal thrust to counter flexural tensile stress (e.g. Zhang *et al* 2024). The difference in ultimate capacity, however, seems to be less when loads are applied eccentrically, where resulting flexural stresses increase.

CONCLUSIONS

The study investigated the response of catenary arches with different span-to-depth aspect ratios (0.35 and 0.60) to concentrated loads at the arch apex and at a distance from it. Two different arch span-to-depth ratios were considered and produced using a steel fibre reinforced concrete mixture. Experimental observations of hinge location and the maximum force that the arches resisted were compared with simple linear elastic analyses, as well as with the extent of vertical deviation between arch geometries and theoretical thrust lines.

Results highlight that catenary arches can resist greater ultimate concentrated loads when applied at the apex than when applied eccentrically. Nevertheless, experimental results in this study suggest that steep arches might be less sensitive to such eccentric loads than shallower arches.

Simple linear elastic analyses appear well-suited to identify locations where successive hinges will form, even beyond elastic limits. The maximum load that catenary arches can resist under concentrated loads is, however, poorly estimated. This might be due to residual flexural stiffness in hinge regions, resulting in non-linear response. It is hypothesised here that simple linear elastic analyses may be more accurate when catenary arches are produced from materials

with lower rotational stiffness at hinge locations. Future investigations should verify this. Moreover, future studies should consider larger sample sizes to better capture variation in structural resistance.

Although simple linear elastic analyses seem well-suited for identifying hinge formation, results highlight the accuracy of simple geometric calculations that account for the extent of vertical deviation between arch geometries and theoretical thrust lines. From a practical design perspective, the results suggest that arch geometries derived solely from self-weight catenary form may not perform optimally where concentrated loads govern. Shallow arches appear more sensitive to eccentric loading and may therefore require greater structural depth or additional reinforcement to resist resulting bending effects. Simple linear elastic analyses can provide a useful first estimate of hinge locations by comparing theoretical thrust-line deviations, though they should not be relied upon to estimate ultimate load capacity.

Although it is hypothesised that the location of hinge formation should also be similar for thinner arch sections (albeit at lower loads), future studies should verify this experimentally.

DATA AVAILABILITY

The results that were analysed in this study can be made available upon reasonable request.

REFERENCES

Allen, E & Zalewski, W. 2009. *Form and forces: designing efficient, expressive structures*. John Wiley & Sons.

Block, P, DeJong, M & Ochsendorf, J. 2006. As hangs the flexible line: Equilibrium of masonry arches. *Nexus Network Journal*, 8(2): 13–24.

Boller, G, Block, P & Schwartz, J. 2024. Heinz Isler's physical form finding of the HIB tennis shells. *Structures*, 65: 106559.

Bradley, R. 2021. Earth brick housing in South Africa: Structural and performance considerations. PhD thesis, University of the Witwatersrand, South Africa.

Bradley, R & Gohnert, M. 2016. Three lessons from the Mapungubwe shells. *Journal of the South African Institution of Civil Engineering*, 58(3): 2–12.

Cvetković, I, Cvetković, A, Popkonstantinović, B & Stojićević, M. 2021. Catenary – its history, significance and application. *Scientific Journal of the Society for Structural Integrity and Life*, 21(2): 191–195.

De Bruin, P D. 1996. The analysis and design of masonry arches. *Journal of the South African Institution of Civil Engineers*, 38(3): 1–4.

Fivet, C & Zastavni, D. 2012. Robert Maillart's key methods from the Salginatobel Bridge design process (1928). *Journal of the International Association for Shell and Spatial Structures*, 53(1): 39–47.

Gáspár, O, Sajtos, I & Sipos, A A. 2023. Multi-hinge failure mechanisms of masonry arches subject to self-weight as derived from minimum thickness analysis. *International Journal of Architectural Heritage*, 17(12): 1921–1949.

Gohnert, M & Bradley, R. 2023. Reinforced concrete beam design using catenary theory. *International Journal of Civil Engineering*, 21(5): 751–762.

Hawkins, W, Orr, J, Shepherd, P & Ibell, T. 2019. Design, construction and testing of a low carbon thin-shell concrete flooring system. *Structures*, 18: 60–71.

Jannasch, E. 2017. Fit forms and free forms of the masonry dome. *Nexus Network Journal*, 19(3): 599–617.

Liu, Z, Zhou, J, Xin, J, Zhuang, Y, Fan, Y & Wang, K. 2025. In-plane bearing capacity analysis of concrete catenary arch with rigid skeleton: test and simulation. *Advances in Bridge Engineering*, 6(1): 10.

Oval, R, Nuh, M, Costa, E, Madyan, O A, Orr, J & Shepherd, P. 2023. A prototype low-carbon segmented concrete shell building floor system. *Structures*, 49: 124–138. Elsevier.

Poleni, G. 1748. *Memorie istoriche della gran cupola del Tempio Vaticano*. Padova.

Prokon Software Limited. 2025. PROKON Version W5.3.04 [Computer Software]. Available: **http://www.prokon.com**.

Rama. 2008. Salginatobel Bridge [Photograph]. Wikimedia Commons, CC BY-SA 2.0 FR.

Weyers, M. 2020. Optimised mix composition and structural behaviour of ultra-high-performance fibre reinforced concrete. Doctoral dissertation, University of Pretoria, South Africa.

Zhang, J M, Wang, C M & Pan, W H. 2024. Methodology for determining optimal design of funicular arches under point loads and self-weight against in-plane buckling. *Engineering Structures*, 300: 117255.

APPENDIX

Derivation of the constant thrust in a catenary arch

The total vertical force over an arch at a distance x: $V(x) = w \cdot x$

$$\tan\theta = \frac{V}{H} = \frac{dy}{dx} = \frac{w}{H} \cdot x$$

$$\frac{d^2y}{dx^2} = \frac{w}{H} = \text{const.}$$

From the geometry of a catenary arch described in Equation 1, it follows that:

$$\frac{dy}{dx} = \sinh\left(\frac{x}{a}\right)$$

$$\frac{d^2y}{dx^2} = \frac{1}{a} \cdot \cosh\left(\frac{x}{a}\right)$$

Since the theoretical thrust is constant, consider the position where $x = 0$:

$$\frac{d^2y}{dx^2} = \frac{1}{a} = \frac{w}{H}$$

$$\therefore H = w \cdot a$$

Derivation of axial force in a catenary arch

From the geometry of a catenary arch described in Equation 1, it follows that:

$$\frac{dy}{dx} = \sinh\left(\frac{x}{a}\right) = \tan\theta$$

$$\cos\theta = \frac{1}{\sqrt{1 + \tan^2\theta}} = \frac{1}{\sqrt{1 + \sinh^2\left(\frac{x}{a}\right)}}$$

At any given location along the arch geometry:

$$N = \frac{H}{\cos\theta} = H \cdot \sqrt{1 + \sinh^2\left(\frac{x}{a}\right)}$$